Geophys. J. Int. (2004) **157,** 515–525 doi: 10.1111/j.1365-246X.2004.02243.x

Shallow crustal structure of Chicxulub impact crater imaged with seismic, gravity and magnetotelluric data: inferences about the central uplift

J. O. Campos-Enríquez,[1] F. J. Chávez-García,[2] H. Cruz,[2] J. G. Acosta-Chang,[3] T. Matsui,[4] J. A. Arzate,[5] M. J. Unsworth[6] and J. Ramos-López[7]

[1] *Instituto de Geofísica, UNAM,* 04510 *Coyoacán, México, D.F, Mexico*
[2] *Instituto de Ingeniería, UNAM,* Apdo. Postal 70-472, *Coyoacán* 04510 *México, D.F, Mexico*
[3] *Departamento de Sismología, CICESE, Ensenada, B.C., Mexico*
[4] *Departament of Earth and Planetary Physics, University of Tokyo, Japan*
[5] *Centro de Geociencias, UNAM, Juriquilla, Qro., Mexico*
[6] *Institute for Geophysical Research, University of Alberta, Edmonton* T6G 2J1, *Alberta, Canada*
[7] *Facultad de Ingeniería, UNAM, Mexico City* 04510, *México, D.F, Mexico*

Accepted 2004 January 12. Received 2003 December 16; in original form 2002 January 21

SUMMARY

The structure of the onshore portion of the Chicxulub impact crater (Yucatan, Mexico) has been studied with seismic, gravity and magnetotelluric (MT) exploration methods. A dispersion analysis of Rayleigh waves along a 150-km long, east–west profile permitted the shallow Tertiary cover to be imaged to a depth of 400 m. Three layers were mapped. The thickness of the first two layers increase as we approach the sinkhole ring from the exterior of the crater (consistent with the existence of a central basin). Those thicknesses change from 100–150 m outside the crater rim to more than 200 m in the terrace zone. At the crater centre, the first layer is again approximately 100 m thick and has a low shear wave velocity (approximately 1 km s^{-1}). Its velocity is slightly larger in the rest of the profile. Outside the central basin, we observed a third layer with a shear wave velocity larger than 1.8 km s^{-1}, but its thickness could not be determined. The velocity distribution along our profile increases monotonously with depth, without low-velocity layers. The inferred inward slope of the two shallow layers immediately outside the central basin correlates well with a smooth gravity gradient. In addition, we present results of detailed gravity measurements along a profile that coincides (in part) with the line covered by the seismic experiment. These gravity measurements were inverted to obtain a density model. In this model (which is of course non-unique), the steep gravity gradients are explained by the faults along which the slumping of the terrace blocks took place. Two of these may correspond to the faults observed at radial distances of 85 and 96 km in offshore seismic data. Finally, we show results obtained using MT soundings. They provide additional, independent constraints on the structure of the Chicxulub crater. MT soundings at the centre of the crater show a sharper increase in resistivity than elsewhere in the impact structure. This sharper increase in resistivity may be related to the uplifted basement of the structural high at a depth of 4 km. Only the MT soundings located over the central gravity high display this feature. Our three different data sets are independently consistent with the existence of a central structural high in the crater and support a twin-peak shape for this high.

Key words: Bouguer gravity, central structural high, Chicxulub impact crater, MT, Rayleigh wave dispersion, sinkhole ring.

1 INTRODUCTION

Based on gravity and magnetic data, Penfield & Camargo (1981) first proposed the existence of an impact structure on the Yucatan peninsula of Mexico. This structure was subsequently linked to the Cretaceous–Tertiary (K/T) boundary mass extinction (Hildebrand & Boyton 1990; Hildebrand *et al.* 1991; Sharpton *et al.* 1992). The Chicxulub crater is the best preserved example of a large terrestrial impact crater. Investigation of its structure is important for an understanding of the mechanism of crater formation and to determine

whether it could have caused a catastrophic disruption of the biosphere. In the last decade, many geological studies have been made, with the aim of mapping the geometry of the impact structure. These studies include drilling (Urrutia-Fucugauchi *et al.* 1996; Rebolledo-Vieyra *et al.* 2000), radiometric and palaeomagnetic dating (Krogh *et al.* 1993; Urrutia-Fucugauchi *et al.* 1994), and petrologic and geochemical studies (Sigurdsson *et al.* 1991; Blum *et al.* 1993; Koeberl 1993). The results have confirmed the K/T age of this structure and also its impact nature.

Geophysical studies have also provided useful information on the shape and dimensions of the Chicxulub impact structure. These studies include gravity and magnetic exploration (Sharpton *et al.* 1993; Pilkington *et al.* 1994; Espíndola *et al.* 1995; Hildebrand *et al.* 1995, 1998; Pilkington & Hildebrand 2000), rock magnetism (Urrutia-Fucugauchi *et al.* 1996), magnetotellurics (Campos-Enríquez *et al.* 1997; Unsworth *et al.* 2002) and heat flow studies (Matsui *et al.* 1998; Flores-Márquez *et al.* 1999). Seismic studies have been used as well, including both active (reflection and refraction seismology and tomography) and passive (using both teleseismic signals and local seismicity) seismology. The highest quality seismic reflection data were collected offshore (Camargo-Zanoguera & Suárez-Reynoso 1994; Morgan *et al.* 1997; Snyder & Hobbs 1999a,b; Brittan *et al.* 1999; Christeson *et al.* 1999; Morgan & Warner 1999a,b). Less extensive onshore seismic studies include a receiver function analysis of teleseismic signals and a dispersion analysis of surface waves (Maguire *et al.* 1998). Seismic reflection studies have confirmed the inference made by previous gravity and magnetics studies of the existence of an approximately 100 km diameter central basin (Pilkington *et al.* 1994; Espíndola *et al.* 1995; Hildebrand *et al.* 1995). The central uplift has been imaged using the refraction seismic method (Christeson *et al.* 2001), tomographic studies based on offshore and onshore seismic data (Morgan *et al.* 2000, 2002), and magnetotelluric studies (Campos-Enríquez *et al.* 1997; Unsworth *et al.* 2002).

The onshore portion of the crater has been studied using primarily gravity and magnetic data, and only limited seismic studies. This paper is a contribution to the understanding of the shallow onshore structure of the crater, in particular of the central structural high. While the existence of this central structural high has been confirmed, its shape and the details of its structure are missing. Our study is based on surface waves, gravity and magnetotelluric data. The surface wave data were obtained from an experiment along a 150 km, east-west profile that crossed the central basin and cenote ring. The dispersion analysis of the surface waves enabled us to establish the shallow seismic velocity structure. The shallow crustal structure of the eastern rim was also determined from detailed gravity measurements. Gravity data proved useful to correlate our study with the structures inferred in offshore seismic studies. They constrain the onshore extrapolation of the offshore seismic reflection crustal images. Finally, the deep structure of the central portion of the crater was studied using magnetotelluric (MT) measurements. All of our results are independently consistent with the existence of a central structural high in the crater and support a twin-peak shape for this high.

Table 1. List of stations that recorded each shot.

Shot	Stations
A1	1, 2
A2	2
A3	3
A4	3, 4, 5
A5	6, 7, 8
A6	9, 10

2 SURFACE WAVE DISPERSION ANALYSIS

2.1 Data collection

A surface wave dispersion study was conducted in 1997 February, along three profiles each approximately 50 km long. The profiles were contiguous and approximately parallel. The composite profile starts in the central part of the crater and runs eastward across the cenote ring (Fig. 1). Explosive charges of 200–250 kg were detonated at depths of 200–250 m in boreholes located at the extremities of each profile. The resulting ground motion was recorded at a number of locations with instrumentation that included both digital and

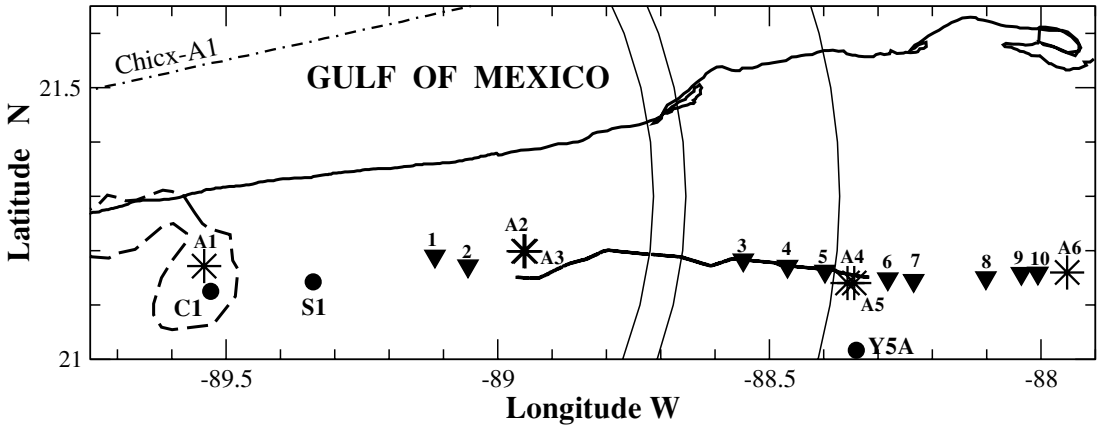

Figure 1. Location of the seismic and gravity experiments. Explosions and receiver locations are shown with asterisks and solid inverted triangles, respectively. Each explosion and receiver are identified using the names given in Table 1. The dashed line outlines the structural high, as obtained from the regional gravity data. The thick, solid line shows the location of the high-resolution gravity profile. The circular arcs represent the projections of the restored rim, normal fault and ring fracture (with reverse blind thrust sense of displacement) mapped on the offshore seismic line (Snyder & Hobbs 1999a,b) at respective radial distances of 85, 96 and 126 km. The location of the offshore seismic line (dash-dotted line marked Chicx-A1, Morgan & Warner 1999a,b) and three deep boreholes drilled in the area (solid circles marked as C1, S1 and Y5A) are shown as reference.

analogue seismographs. The digital instruments were four Scintrex PRS-4 seismic recorders (coupled to 1 Hz LE-3-D Lennartz seismometers), four SSR-1 Kinemetrics recorders (coupled to WR-1 Kinemetrics seismometers) and six DCS-302 Terra Technology recorders (coupled to 1 Hz L4 Mark seismometers). The analogue seismographs were Sprengnether MEQ800 instruments coupled to 1 Hz Ranger sensors produced by Kinemetrics. The survey layout is shown in Fig. 1.

At several sites we had excessive background noise. However, several records showed very clear arrivals in the vertical component, which are well correlated with the corresponding radial component. These arrivals were identified as Rayleigh waves excited by the explosions in the superficial stratigraphy. Transverse components do not show significant surface wave arrivals, as is expected for an explosive source. Al-Eqabi & Herrmann (1993), Jongmans & Demanet (1993), Chávez-García *et al.* (1995) and Ramos-Martínez *et al.* (1997) have shown that the inversion of surface wave dispersion curves can be used to determine the elastic properties of shallow crustal structure. In this approach, each record may be considered independently. This is important because the useful records have irregular spacing. Thus, we selected the highest quality records, where surface waves were readily apparent, to determine group velocity dispersion curves. When timing for the record is not available, it is not possible to determine absolute velocities. However, if Rayleigh waves can be identified, it is possible to determine a relative dispersion curve. Absolute velocity values may be assigned by comparing the shape of the resulting dispersion curve with that obtained from neighboring records.

2.2 Data analysis

The selected records were analysed using the multiple filtering technique (MFT) of Dziewonski *et al.* (1969) as implemented by Herrmann (1987). Fig. 2 shows, for example, a diagram of the energy distribution in the group velocity–frequency (U–f) plane for the vertical component of the record obtained at site 5 for explosion A4, 5 km away. The largest amplitudes in the record correspond to a Rayleigh wave pulse arriving at the station with a group velocity between 0.75 and 1 km s^{-1} in the frequency band 1 to 7 Hz. We determined group dispersion from both vertical and radial components for a total of 17 records. Fig. 3 shows an example of the dispersion curves determined from these records. The results are consistent indicating that our dispersion curves are reliable. Finally, the group velocity dispersion curves were inverted for thickness and shear wave velocity in a layered structure. The inversion programme of Herrmann (1987) was used with stochastic damping. Less than 10

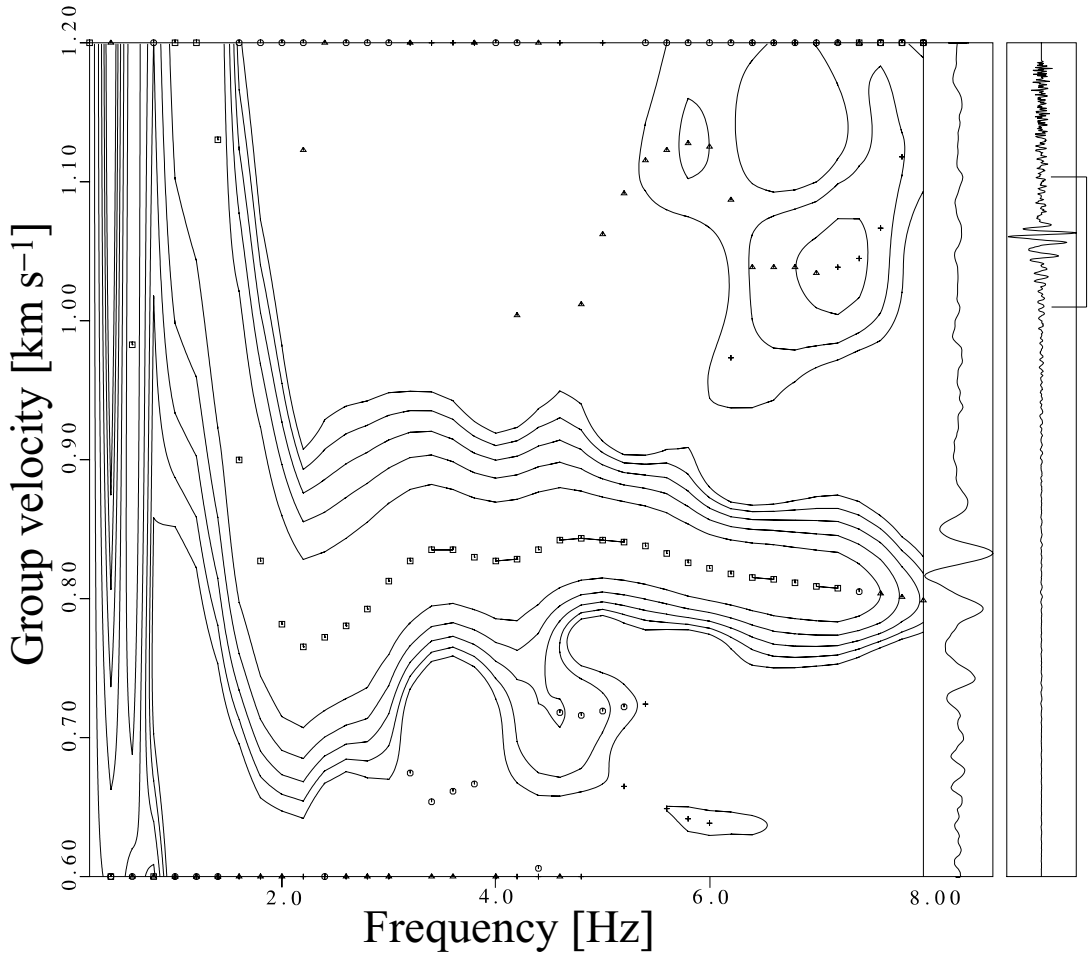

Figure 2. Example of the energy distribution in the group velocity–frequency (U–f) plane. This diagram corresponds to the vertical record obtained at station 5 from shot A4, 5 km away. The rightmost trace (plotted downward) shows the recorded signal, with the prominent Rayleigh wave pulse indicated. Immediately to the left, the same trace is shown, plotted as a function of group velocity. The group velocity range of the plot allows to plot only the portion of the complete trace indicated with the square bracket. The contours in the diagram show that this Rayleigh pulse arrives at the station with a group velocity approximately 800 m s^{-1}. The symbols in the diagram indicate the location of the four largest amplitudes for each frequency value.

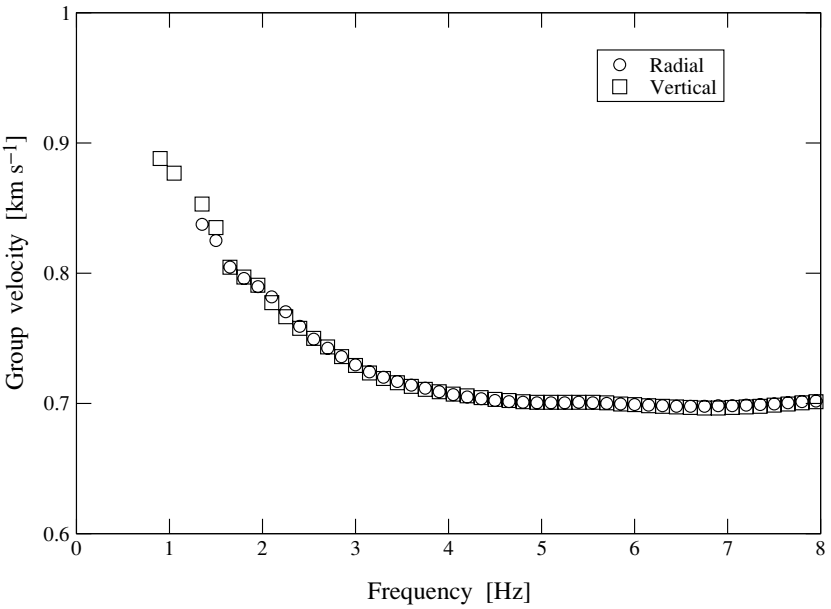

Figure 3. Example of dispersion curves obtained from the analysis of the vertical and radial components. These curves were obtained using the record of shot A2 at site 2. We observe the very good agreement between radial and vertical components, required by Rayleigh waves. Our results have a good resolution between 1 and 4 Hz.

iterations were required to obtain a satisfactory fit between observed and computed dispersion. Given the limited frequency range in our records, the maximum depth for which the resolution of the models was adequate is between 150 and 400 m. However, in all cases, the half-space velocity has low resolution.

Direct interpretation allows us to determine an average group velocity between the source and each station. However, it is also possible to obtain additional, more detailed information. Consider an explosion recorded by two adjacent stations. If we assume that the station closer to the source gives a reliable measure of average group velocity between the source and that station, the differences between the dispersion curves determined for the two stations can be mapped to the medium between them (Shapiro *et al.* 1997). An example is shown in Fig. 4. In this figure, we show the group velocity dispersion curves obtained between shot A4 and three stations (3, 4, and 5). For example, the difference between the curves for stations 3 and 4, A4-3 and A4-4, respectively, allowed the computation of a group velocity dispersion curve for the interstation interval between sites 3 and 4, labelled IS3-4 in the figure. After inversion of the group velocity dispersion curves, we can map the resulting shear wave velocity versus depth profiles to the interval between adjacent stations, as shown schematically in the lower diagram of Fig. 4.

Fig. 4 does not show error bars for shear wave velocities or thickness of the models. The reason is that it is not straightforward to map the uncertainties of the group velocity estimates on the uncertainties of the parameters of the final models. For this reason, in order to estimate the uncertainties of those parameters, we have used a Monte Carlo approach. We simulated a large number of velocity profiles, starting from our final models, considering some variation about the final shear wave velocity and thickness values. Then, we computed the expected group velocity dispersion for each of those profiles. Finally, the comparison of the forward modelled dispersion curves with those estimated from the seismic data allowed us to determine uncertainties for the parameters of our inverted models. The uncertainties for the parameters of the topmost layer (thickness and shear wave velocity) are comprised between 5 and 10 per cent of the final values. For the velocity profiles that have three layers, the intermediate layer has uncertainties between 10 and 15 per cent. Finally, in all cases, the half-space shear wave velocity has an uncertainty of approximately 20 per cent.

2.3 Results

The final result is a sequence of layered models that represents the shallow structure between the sources and stations, or between adjacent stations (Fig. 5). The first two velocity profiles cover the distance between boreholes A1 and A2/A3, and correspond to the centre of the crater (including the peak ring and the structural high). The structure between 60 and 100 km from the centre of the crater is sampled by only one record. This part corresponds to the outer segment of the central basin (terrace zone) as well as a section outside the crater rim. The following depth–velocity profiles are associated with the distance intervals 103–111, 111–116, 116–121 and 121–133 km respectively, and sample the shallow structure outside the central basin (Fig. 1).

For most of the records analysed, the velocity distribution can be determined from the surface to a depth of 200–300 m. In one case, the depth of investigation reached 400 m. For the two outer depth–velocity profiles, the maximum depth investigated was only 150 m. The thickness of the first layer increases, as we approach the central basin, changing from less than 100 m immediately outside the central basin to more than 200 m in the terrace zone. According to the first two depth–velocity profiles, the topmost layer is again approximately 100 m thick in the central portion of the crater. At the centre of the crater this layer has low shear wave velocity (approximately 1 km s^{-1}). This velocity is slightly larger in the rest of the profile, but always less than 1.2 km s^{-1}. The shear wave velocity of the second layer varies between 1.1 and 1.5 km s^{-1}. This layer also shows an increase in thickness as we approach the central basin: the thickness changes from approximately 150 m outside the rim up to 200 and 250 m in the vicinity of the rim. In the central part

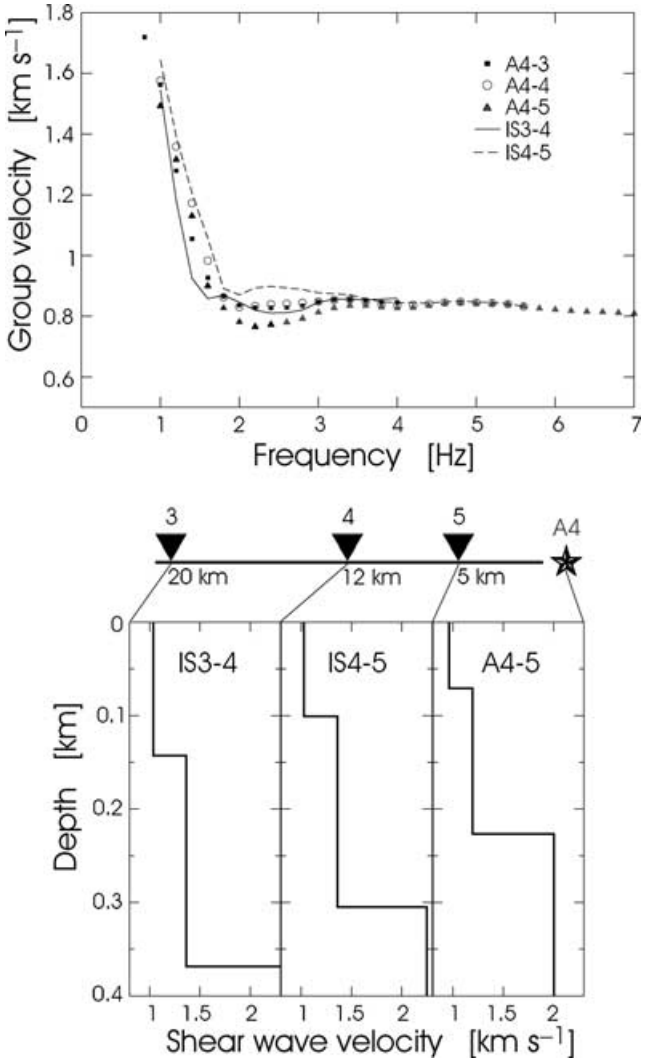

Figure 4. Example of how the differences in group velocity dispersion from contiguous stations are mapped to the space between the stations. The top diagram shows the group velocity dispersion curves, as a function of frequency, determined for the three stations (3, 4 and 5) that recorded shot A4. Each symbol corresponds to the group velocity determined from each record (e.g. solid squares for the interval between A4 and station 3). The solid line indicates the group velocity dispersion curve obtained by difference between stations: IS3-4 and IS4-5 for the interstation intervals between stations 3 and 4, and 4 and 5, respectively. The lower diagram shows the depth shear wave velocity profiles inverted from the group velocity dispersion curves. Above these profiles, a schema shows the relative position of the receivers (solid triangles, the corresponding source-station distance is given below each receiver) and the source (star). Each velocity profile has been labelled to identify it with the interval to which it is mapped.

of the crater the thickness of this second layer is not defined. The velocity of the second layer is lower at the crater centre than outside. Results from reflection seismic method have shown that the stratigraphic sequence is not flat in the basin: the western basin filled in first, then the eastern basin and finally the central basin. The central basin may have started a few hundred meters higher than the zone outward from the peak ring in the annular trough, but it clearly did not stay as a topographic high for very long. The lower velocity of the second layer at the centre of the crater may reflect the younger age of the central basin sediments. A second possibility is that this second layer has undergone dolomitization of carbonates at the centre of the crater, resulting in a higher porosity. The third layer was only observed outside the central basin. It has a velocity higher than 1.8 km s^{-1} but its thickness could not be determined.

The thickness increase of the first two layers as we approach the sinkhole ring from outside is consistent with the existence of a central basin. These layers show a gentle dip towards the centre of the basin. The depth–velocity profile at the easternmost portion of the profile implies that the first layer gets thicker eastward. All our shear wave velocity profiles show velocity increasing with depth, consistent with the results of the downhole seismic experiment by Cué (1953), however, we were not able to correlate our results with available geological data on the Tertiary strata of the zone.

Maguire *et al.* (1998) and Mackenzie *et al.* (2001) report an inverted velocity gradient in the upper 300 m of the crater sediments, outside a circular region across the crater centre. We do not observe such a low-velocity layer along our profile. However, most of the event-station paths analysed by those authors are located away from our profile and only two of their stations are close to it (near our boreholes A2 and A3). For these two stations, Maguire *et al.* (1998) and Mackenzie *et al.* (2001) do not report the seismic velocity inversion. Thus, the area where the low-velocity inversion is observed is limited either to: (i) the west and south of the crater centre, but not to the east of it; or (ii) a ring (associated with an annular gravity low) around the central structural high. The first possibility implies a lack of radial symmetry in the velocity structure of the shallow Tertiary cover. An imperfect radial symmetry of the crater can be readily identified in the regional Bouguer anomaly map (De La Fuente *et al.* 1992; Sharpton *et al.* 1993; Campos-Enríquez *et al.* 1998; Hildebrand *et al.* 1998).

3 GRAVITY

To complement the seismic study, we conducted detailed gravity measurements along the road parallel to our profile (Fig. 1). We used a Scintrex MicroGal-Autograv digital gravimeter, with measurements every 200 m, tied to the gravity base at the airport in Merida. Because the equipment is temperature compensated there was no drift in the measurements. A reference density of 2670 kg m^{-3} was used and the complete Bouguer anomaly was obtained (i.e. free-air, latitude, Bouguer and terrain corrections out to 20 km were applied). We used the 1984 International Gravity Formula. Fig. 6 shows the Bouguer anomaly obtained.

The detailed gravity profile is 64 km long, covers the second refraction line between boreholes A3 and A4 and crosses the cenote ring. The long wavelength features of the measured Bouguer anomaly agree well with the gravity signature of the Chicxulub crater. However, the new data have considerably more detail. Fig. 6 compares the results of the detailed gravity profile with the corresponding section of the regional gravity map (De La Fuente *et al.* 1992). A conspicuous feature in the detailed profile is the existence of a local gravity high located immediately outside the basin rim. This gravity high is quite distinct and corresponds to an area where the cenotes are not distributed in a narrow ring (as in the western rim) but in a wider belt. The relative gravity low immediately to the east could be associated with a fracture zone.

Similar gravity highs are less conspicuous (but it is still possible to identify them) in the closely spaced (0.5–3 km) measurement profiles reported by Hildebrand *et al.* (1995) for the western portion of the crater. Here, a series of small amplitude (approximately 2 mGal) negative anomalies are mounted on the gravity highs. The differences in the shape of these local gravity highs between the

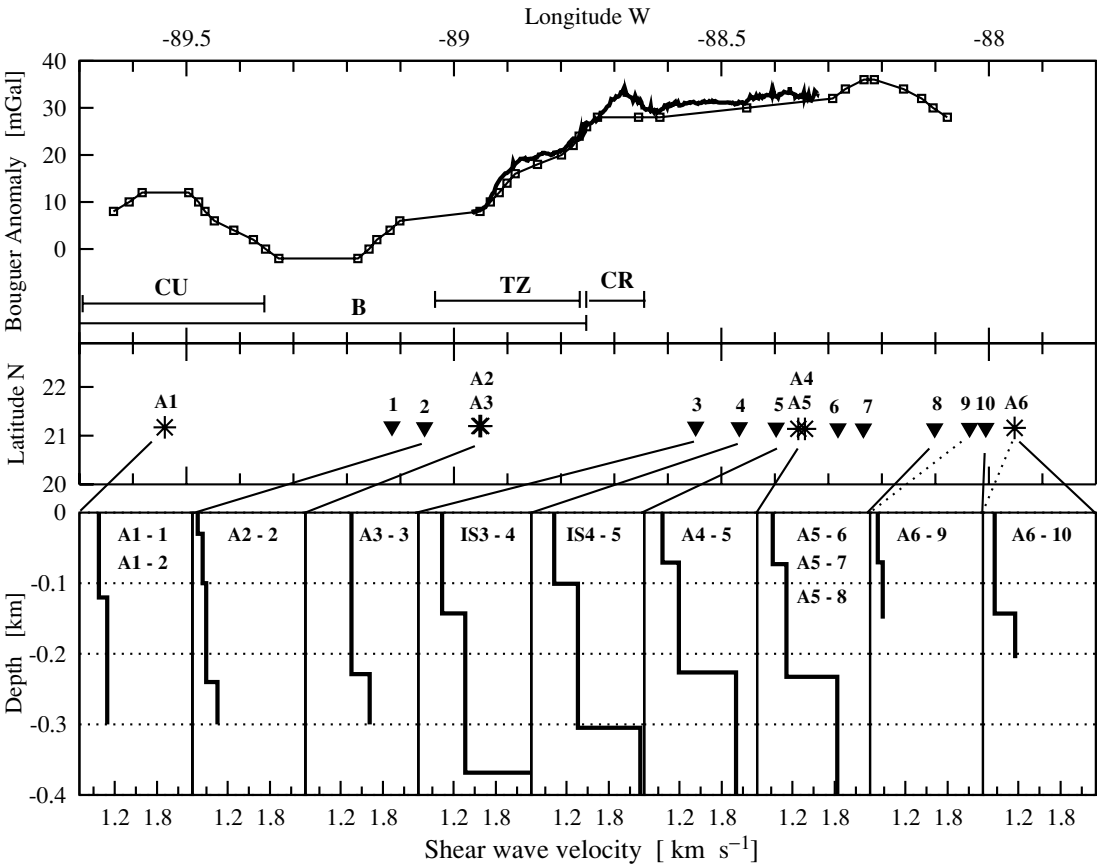

Figure 5. Depth–velocity profiles obtained from the seismic experiment. The top diagram shows the Bouguer anomaly obtained from the regional gravity map and our detailed gravity profile (shown in more detail in Fig. 6), for comparison purposes. The lines and letters below the gravity profile indicate the location of the different features of the crater: B stands for basin, CU for central uplift, CR for Cenote ring and TZ for terrace zone. The middle diagram gives the location of the receivers and shots of the seismic experiment. The lower diagrams give the final shear wave velocity profiles obtained from the seismic experiment. The lines connecting the middle and lower diagrams indicate to which segment of the total profile each velocity profile corresponds.

eastern and western sectors suggests minor structural changes of the crater with azimuth.

We have inverted our gravity profile to obtain a plausible density model (Fig. 7). The density values used were measured from samples of borehole cores from Chicxulub. Our density values agree with those used by other authors (e.g. Hildebrand *et al.* 1995; Vermeesch & Morgan 2004). Our model is based on that of Hildebrand *et al.* (1995). The steep gravity gradients are accounted for by faults (labelled 1 and 2 in Fig. 7) along which the slumping of the terrace blocks took place. Two of these faults may correspond to the restored rim and the normal fault observed at radial distances of 85 and 96 km on the Chicx-A1 offshore seismic line (Snyder & Hobbs 1999a,b). Our model shows two additional faults (labelled 3 and 4 in Fig. 7).

4 MT DATA

Magnetotellurics has been used previously to explore the structure of Chicxulub crater. Campos-Enríquez *et al.* (1997) analysed 10 soundings. They detected a 1 to 2 km thick layer of low-resistivity crater fill. One of their MT soundings suggested the presence of a high resistivity central structural high. Unsworth *et al.* (2002) used 30 additional MT soundings to image the electrical resistivity structure of the impact crater. Their results showed a region of high resistivity in 20 of their MT soundings, located at the crater centre. That region was interpreted as the central uplift.

In this paper, we present the results of analysing an additional 18 MT soundings. The central part of the crater was covered by seven soundings (five of them on the outline of the structural high), while an additional 11 were measured along a N–S section (Fig. 8). These new soundings had the objective of obtaining additional detail of the structure of the central uplift, already imaged previously. Horizontal and vertical electric and magnetic natural electromagnetic fields were measured. The time length of the measuring window was between 16 and 24 hr. The frequency range measured was from 384 to 5.5×10^{-5} Hz. Data processing followed the lines described in Unsworth *et al.* (2002).

The results show a decrease in apparent resistivity from the surface downward, as the MT signals penetrate the low-resistivity crater fill, in the frequency range 100 to 0.3 Hz. As the frequency decreases further, from 0.3 to 0.001 Hz, the resistivity rises, reflecting the resistive basement. All our MT data exhibit this basic pattern. However, significant differences can be observed. Apparent resistivity as a function of frequency for those MT soundings located over the central structural high have a slighter apparent resistivity decrease from 100 to 0.3 Hz and a sharper rise in the resistivity for frequencies smaller than 0.3 Hz, than elsewhere within the impact structure. Fig. 9 shows, for example, the apparent resistivity as a function of frequency for two MT soundings: site 24 (located over

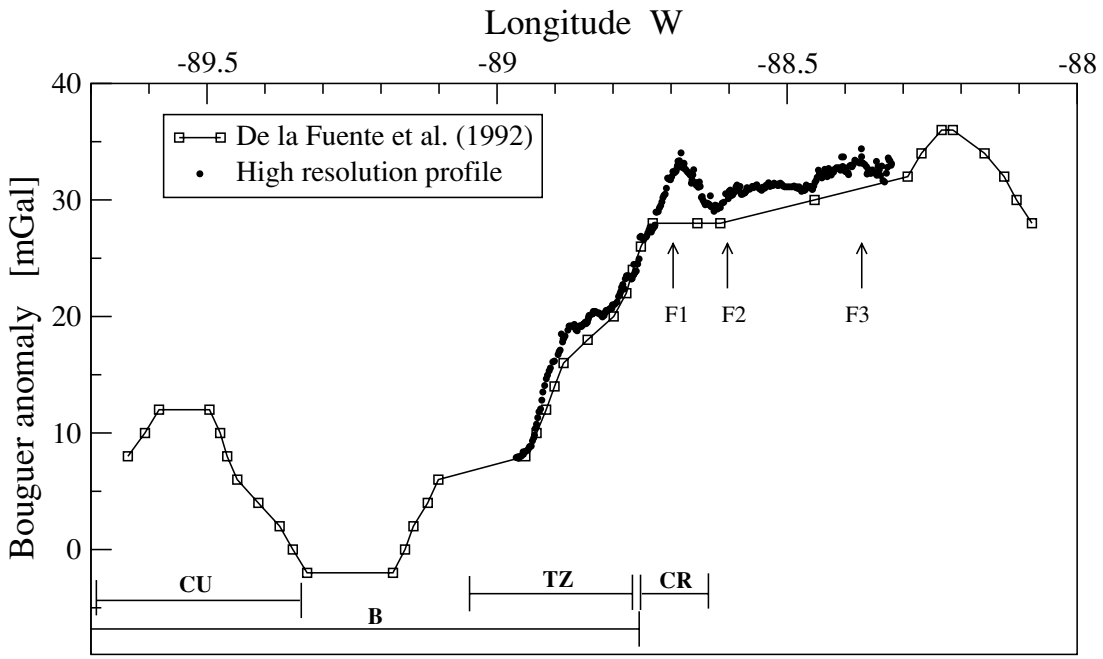

Figure 6. Bouguer anomaly along our high-resolution gravity profile. The location of the measurement profile is shown in Fig. 1. The gravity profile read from the regional Bouguer anomaly map for Yucatan (De La Fuente *et al.* 1992) is also shown. The lines and letters below the gravity profile indicate the location of the different features of the crater: B stands for basin, CU for central uplift, CR for Cenote ring and TZ for terrace zone. The arrows represent the projections of the restored rim (F1), the normal fault (F2) and the ring fracture (F3) (with reverse blind thrust sense of displacement) mapped on the offshore seismic line (Snyder & Hobbs 1999a,b) at respective radial distances of 85, 96 and 126 km.

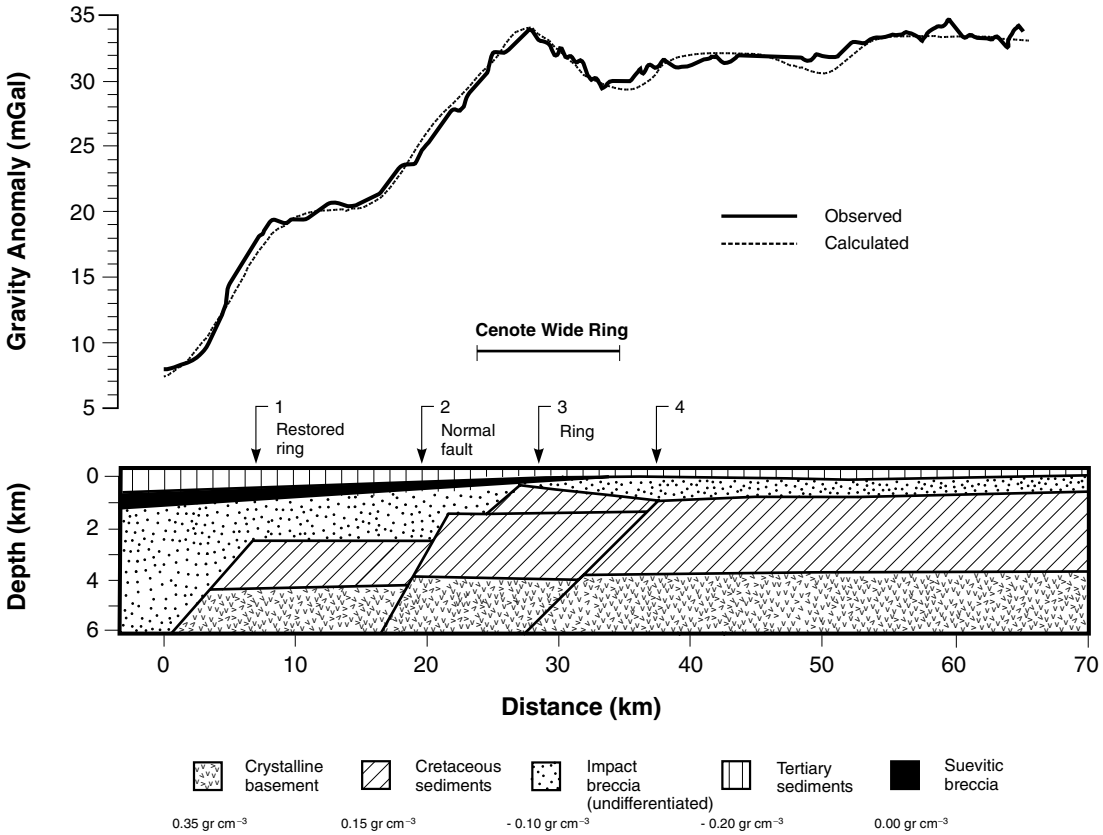

Figure 7. Density model inverted from the high-resolution gravity profile (Fig. 6). Densities are given in g cm^{-3}. Reference density in this figure in 2.3 g cm^{-3}. Numbers on the figure indicate faults. The location of the measurement profile is shown in Fig. 1.

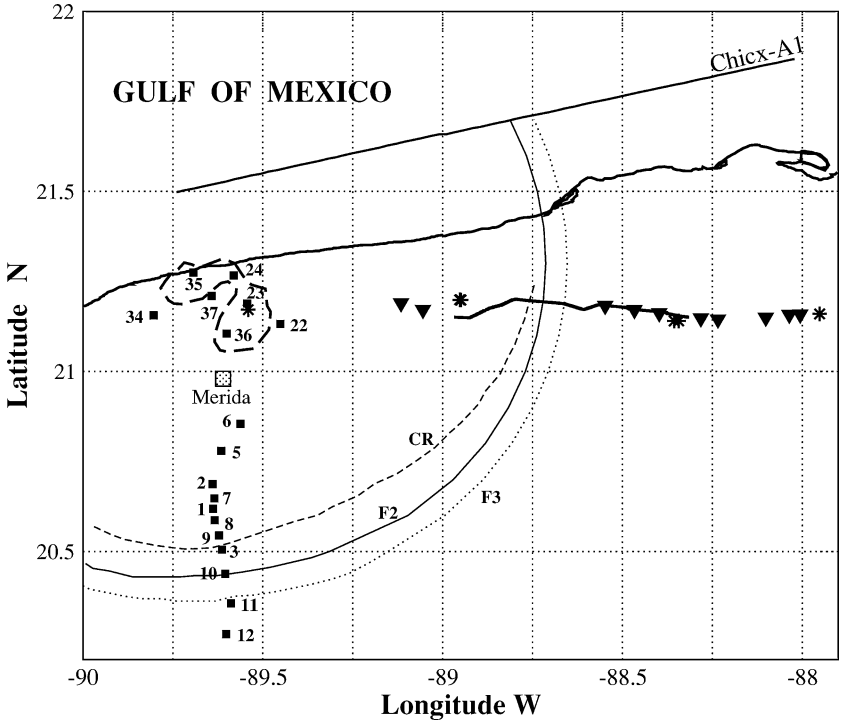

Figure 8. Location map of the MT experiment. The locations of the MT soundings are shown with solid squares. The dashed line outlines the structural high, as obtained from the regional gravity data. The locations of our seismic profile and the detailed gravity profile are shown, using the same symbols as in Fig. 1, for reference. The circular arcs represent the cenote ring (dashed line, marked CR), the projections of the restored rim (solid line, marked F2) and the normal fault (dotted line, marked F3) mapped on the offshore seismic line (Snyder & Hobbs 1999a,b). The location of the offshore seismic line (thick solid line marked Chicx-A1, Morgan & Warner 1999a,b) is also shown as reference.

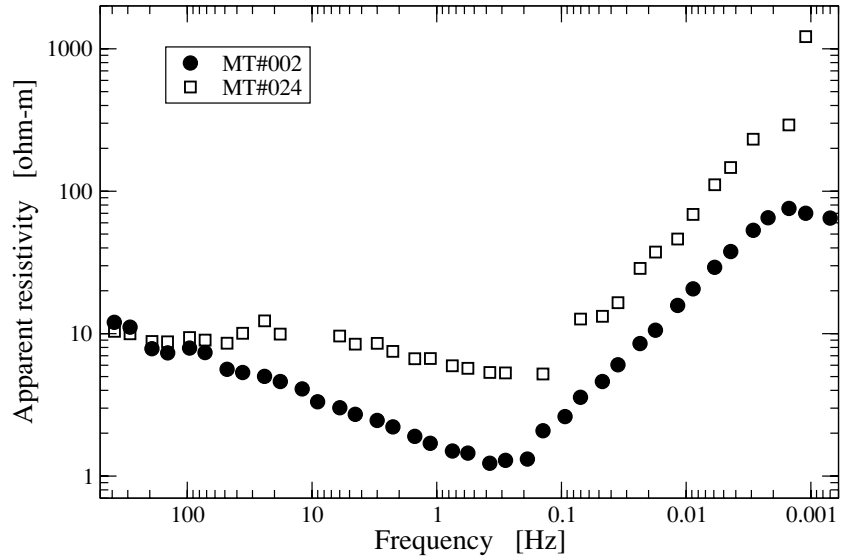

Figure 9. Example of the different depth electrical resistivity behaviour for MT soundings above the crater centre and elsewhere. Apparent resistivity as a function of frequency for two MT soundings over the Chicxulub impact structure. Sites 2 and 24 are located at radial distances of approximately 60 and 0 km.

the central structural high) and site 2 (at a radial distance of 60 km of the crater centre). The slope of apparent resistivity as a function of frequency is larger for site 24 than for site 2 for frequencies smaller than 0.1 Hz. Thus, the response of the MT soundings seems to be influenced by their position in relation to the central gravity high.

Large apparent resistivities may have several explanations. Well log information indicates that beneath the Tertiary cover lies a unit of impact breccia (Rebolledo-Vieyra *et al.* 2000). The suevitic breccia has a high magnetic susceptibility, and a high resistivity. Seismic studies have mapped a 1 km thick unit with low velocities and densities below the Tertiary cover, that has been interpreted as solidified melt rocks (suevitic breccia with isolated melt pods or suevitic breccia overlying a coherent melt sheet). It is possible that the melt sheet may blanket the top of the structural high. The large resisitivities we observe may therefore be the result of the suevitic breccia, or the melt rocks. However, the lateral extension of these two formations

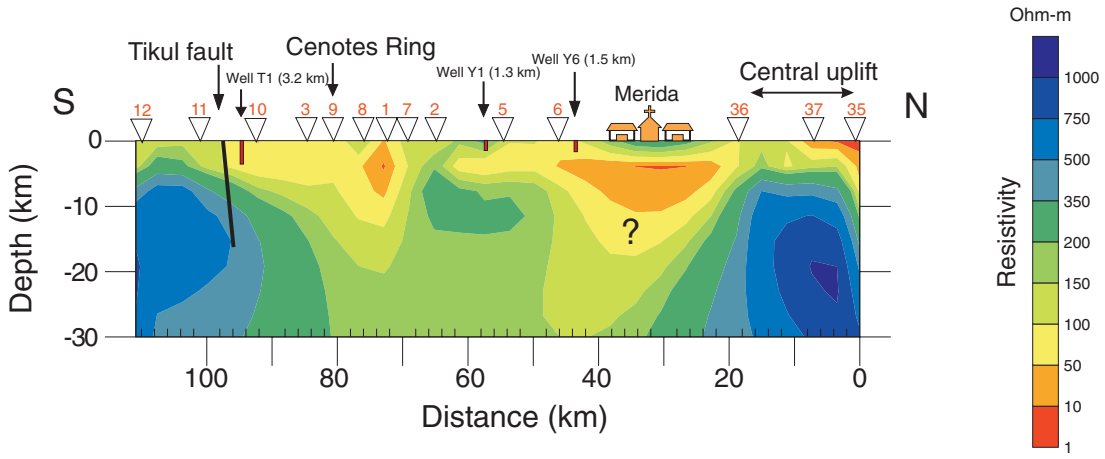

Figure 10. Inverted depth resisitivity profile from the north–south line of MT measurements. The open triangles indicate the location on the profile of the measurements. The central uplift is clearly shown in this figure. The projections on this section of wells T1, Y6 and Yaxcopiol-1 (Urrutia-Fucugauchi *et al.* 2001) are shown as reference.

are wider than the restricted region where we observe steeper resistivities with decreasing frequency. For this reason, our preferred explanation for this feature is that the basement has been uplifted and the feature reflects the structural high. Fig. 10 shows the inverted resistivity section obtained from our MT soundings along the N–S profile. According to this figure, the structural high has a diameter of approximately 40 km, with the top at a depth of 4 km.

5 DISCUSSION

The existence of the structural high, at the crater centre, has been shown mainly from gravity and magnetic studies. It is only recently that seismic data, combining offshore and onshore studies, have succeeded in providing an image of the central uplift. The shape of this structure, however, is still a matter of controversy. While gravity shows a twin-peak structure (e.g. Espíndola *et al.* 1995; Pilkington & Hildebrand 2000), the tomographic images of Morgan *et al.* (2002) suggest a concave shape for the top of the structural high.

We have presented results of three different geophysical methods, applied to the exploration of the Chicxulub crater. Each of these methods independently provide some constraints on this structure. It is difficult to correlate the results among them, not only because each method measures a different physical property, but also because the resolution differed significantly among the methods. Analysis of surface wave dispersion allowed us to constrain the superficial structure (down to 300–400 m) in terms of shear wave velocity. Gravity measurements allowed us to obtain an inverted density model, with good resolution in the depth range 0–4 km. Finally, MT soundings allowed us to determine the resistivity properties of the structure of the crater in the range 0–30 km.

The analysis of group velocity dispersion along our seismic profile allowed us to map two to three layers. The thickness of the first two layers increase as we approach the sinkhole ring from the exterior of the crater, changing from 100–150 m outside the crater rim to more than 200 m in the terrace zone. At the crater centre the first layer is again approximately 100 m thick and has a low shear wave velocity (approximately 1 km s^{-1}). Our profiles do not show velocity inversions, as found by Maguire *et al.* (1998) for similar radial profiles but along different directions from the crater's centre. This is definitely a good indication of an asymmetrical structure for the Tertiary cover. Notwithstanding the very different scales, the inferred inward slope of the two shallow layers immediately outside the central basin correlates well with a smooth gravity gradient. Our final density profile also shows an increase of the sedimentary layers towards the centre. Thus, it seems as though the structure of the superficial layers is conditioned by the deeper structure or at least parallels it. If we accept this, then the lack of symmetry shown in the Tertiary cover suggests that the asymmetrical structure revealed by the regional gravity and magnetic studies reflects itself throughout the complete stratigraphic sequence.

The previous results are complemented, in a way, with the results from our MT soundings. Although constraints in the field imposed a different direction for our profile, relative to the seismic and gravity lines, the results also support the presence of a high-resistivity central uplift in the basin, at the centre of the crater. The depth scale sampled by MT is very different from that sampled by previous methods. However, it allows us to characterize the differences in the variation of apparent resistivity with frequency between sites over the central uplift and elsewhere. The final resistivity section illustrates the large-scale resistivity structure of the crater and shows clearly the shape and size of the central uplift. This image is entirely consistent with images of this structural high obtained previously with seismic methods. The central uplift has a diameter of approximately 40 km and its top is located at a depth of approximately 4 km.

Finally, the results of all three exploration methods are consistent with the presence of the structural high. Unfortunately, our results lack the resolution to constrain its shape. However, the correlation of our results with those published previously do indicate that the shape of the structural high lacks symmetry. Thus, they favour a twin-peak shape for the central uplift. This is in apparent contradiction to the concave shape preferred from the interpretations of tomographic studies. However, this apparent contradiction would be solved if the rim of the concave central uplift is irregular. Final solution of this point requires additional, more detailed studies of this feature of the Chicxulub crater.

6 CONCLUSIONS

We have studied the structure of the Chicxulub crater using three independent geophysical methods. Surface wave dispersion and a detailed gravity profile were measured along an east–west line, from

the crater centre to the cenote ring. In addition, a north–south profile was covered with MT measurements, seven of which were on the structural high, or very close to it.

Based on the dispersion analysis of Rayleigh waves, we determined the depth–velocity profile of the shallow Tertiary cover along the profile. The Tertiary cover was sampled down to depths between 200 and approximately 400 m. The inversion of group velocity dispersion curves allowed us to determine the shear wave velocity structure, which consists of two or three layers. The thickness of the first layer increases towards the central basin, from less than 100 m immediately outside, to more than 200 m in the terrace zone. The second layer also thickens towards the centre of the impact basin, from about 150 m outside the rim to 200 and 250 m close to the rim. In the central portion of the crater, the bottom of this second layer was not reached.

The increase in thickness of the first two layers as we approach the sinkhole ring from the exterior of the crater is consistent with the existence of a central basin. The difference in seismic velocity in the first layer at the crater centre and at the rim (and outside the crater) can be the result of either a younger age of the central basin sediments (consistent with a central structural high), or perhaps of a dolomitization of carbonates leading to a higher porosity. Our velocity profiles do not show a low-velocity layer determined in previous studies. This supports an asymmetrical shape for the central structural high.

The structure of the Tertiary cover determined from the seismic experiment is consistent with the deeper structure obtained from the inversion of a detailed gravity profile. The inferred inward slope of the two shallow layers immediately outside the central basin is reflected in the gravity data by a regionally smooth gradient. The inverted density model (one of the different possible models compatible with our data) bears similarities to that of Hildebrand *et al.* (1995). The steep gravity gradients are accounted for by faults along which the slumping of the terrace blocks took place. In our model, additional faults delimit the relative gravity highs.

Finally, we collected MT data along a north–south profile, with seven soundings on or very close to the structural high (as determined from regional gravity measurements) and eleven additional soundings extending some 100 km from the centre of the crater. Although the nature and scale of the results from the MT measurements are very different from our previous results, a coherent picture emerges. Results from the MT, image clearly the structural high. They indicate a diameter of 40 km for this feature and indicate that its top is buried at approximately 4 km depth.

The results of all three exploration methods we have used are consistent with the presence of the structural high. Unfortunately, our results lack the resolution to constrain its shape. However, the correlation of our results with those published previously, indicate that the shape of the structural high lacks symmetry. They also suggest that the deeper structure is paralleled by the Tertiary cover. Our results favour a twin-peak shape for the central uplift. This is in apparent contradiction to the concave shape preferred from the interpretations of tomographic studies. However, this contradiction would be solved if the rim of the concave central uplift is irregular. Final solution of this point requires additional, more detailed studies of this feature of Chicxulub crater.

ACKNOWLEDGMENTS

The comments of Dr J. Morgan and one anonymous reviewer significantly improved the manuscript. This research was partially supported by CONACYT, Mexico, under Contract 32588-T, NISSAN Foundation and the Panamerican Institute of Geography and History, project 01-62. We acknowledge support for fieldwork from Instituto de Ingeniería, UNAM. Adriana Campos assisted in the preparation of the drawings.

REFERENCES

Al-Eqabi, G.I. & Herrmann, R.B., 1993. Ground roll: a potential tool for constraining shallow shear wave structure, *Geophysics,* **58,** 713–719.

Blum, J.D., Chamberlain, C.P., Hignston, M.P., Koeberl, C., Marin, L.E., Schuraytz, B.C. & Sharpton, V.L., 1993. Isotopic comparison of K/T boundary impact glass with melt rock from the Chicxulub & Manson impact structures, *Nature,* **364,** 325–327.

Brittan, J., Morgan, J., Warner, M. & Marín, L., 1999. Near-surface seismic expression of the Chicxulub impact crater, in *Large Meteorite Impacts and Planetary Evolution,* Vol. 339, pp. 269–279, eds Dressler, B. & Sharpton, V., Spec. Pap. Geol. Soc. Am., Boulder, CO.

Camargo-Zanoguera, A. & Suárez-Reynoso, G., 1994. Evidencia sísmica del cráter de impacto de Chicxulub, *Boletín de la Asociación Mexicana de Geofisicos de Exploración,* **34,** 1–28.

Campos-Enríquez, J.O., Arzate, J.A., Urrutia-Fucugauchi, J. & Delgado-Ramírez, O., 1997. The subsurface structure of the Chicxulub crater (Yucatan, Mexico): preliminary results of a magnetotelluric study, *The Leading Edge,* **16,** 1774–1777.

Campos-Enríquez, J.O., Morales-Rodríguez, H.F., Domínguez-Mendez, F. & Birch, F.S., 1998. Gauss's theorem, mass deficiency at Chicxulub crater (Yucatan, Mexico), and the extinction of the dinosaurs, *Geophysics,* **63,** 1585–1594.

Chávez-García, F.J., Ramos-Martínez, J. & Romero-Jiménez, E., 1995. Surface wave dispersion analysis in Mexico City, *Bull. seism. Soc. Am.,* **85,** 1116–1126.

Christeson, G.L., Buffler, R.T. & Nakamura, Y., 1999. Upper crustal structure of the Chicxulub impact crater from wide-angle ocean bottom seismograph data, in *Large Meteorite Impacts and Planetary Evolution,* Vol. 339, pp. 291–298, eds Dressler, B. & Sharpton, V., Spec. Pap. Geol. Soc. Am., Boulder, CO.

Christeson, G.L., Nakamura, Y., Buffler, R.T., Morgan, J. & Warner, M., 2001. Deep crustal structure of the Chicxulub impact crater, *J. geophys. Res.,* **106,** 21 751–21 769.

Cué, A.V., 1953. Determinación de velocidades sísmicas en el pozo Chicxulub No. 1, *Boletín de la Asociación Mexicana de Geológos Petroleros,* **5,** 285–290, (in Spanish).

De La Fuente, M., Mena, M. & Aiken, C.L.V., 1992. *Cartas gravimétricas de la República Mexicana, I. Carta de la Anomalía de Bouguer,* INEGI, México.

Dziewonski, A.M., Bloch, S. & Landisman, M., 1969. A technique for analysis of transient seismic signals, *Bull. seism. Soc. Am.,* **59,** 427–444.

Espíndola, J.M., Mena, M., de la Fuente, M. & Campos-Enríquez, J.O., 1995. A model of the Chicxulub impact structure (Yucatan, Mexico) based on its gravity and magnetic signatures, *Phys. Earth planet. Int.,* **92,** 271–278.

Flores-Márquez, E.L., Chávez-Segura, R.E., Campos-Enriquez, J.O. & Pilkington, M., 1999. Preliminary 3-D structural model from the Chicxulub impact crater and its implications in the actual geothermal regime, *Trends in Heat, Mass and Moment Transfer,* **5,** 19–40.

Herrmann, R.B., 1987. *Computer programs in seismology,* Vol. 8, St. Louis University, St. Louis, MO.

Hildebrand, A.R. & Boyton, W.V., 1990. Locating the Cretaceous/Tertiary boundary impact crater(s), *EOS, Trans. Am. geophys. Un.,* **71**, Fall Meet. Suppl., 1429.

Hildebrand, A.R., Pilkington, M., Connors, M., Ortiz-Alemán, C. & Chávez, R.E., 1995. Size and structure of the Chicxulub crater revealed by horizontal gravity gradients and cenotes, *Nature,* **376,** 415–417.

Hildebrand, A.R., Penfield, G.T., Pilkington, M., Camargo, A., Jacobsen, S.B. & Boyton, W.V., 1991. Chicxulub crater: A possible Cretaceous/Tertiary boundary impact crater on the Yucatan Peninsula, Mexico, *Geology,* **19,** 867–871.

Hildebrand, A.R. *et al.*, 1998. Mapping Chicxulub crater structure with gravity and seismic reflection data, in *Meteorites flux with time and impact effects,* Vol. 140, pp. 177–193, eds Grady, M.M.,*et al.,* Geological Society, London, Special Publications.

Jongmans, D. & Demanet, D., 1993. The importance of surface waves in vibration studies and the use of Rayleigh waves for estimating the dynamic characteristics of soils, *Engineering Geology,* **34,** 105–113.

Koeberl, C., 1993. Chicxulub crater, Yucatan: tektites, impact glasses, and the geochemistry of target rocks and breccias, *Geology,* **21,** 211–214.

Krogh, T.E., Kamo, S.L., Sharpton, V.L., Marín, L. & Hildebrand, A.R., 1993. U-Pb ages of single shocked zircons linking distal K/T ejecta to the Chicxulub crater, *Nature,* **366,** 731–734.

Mackenzie, G.D., Maguire, P.K.H., Denton, P., Morgan, J. & Warner, M., 2001. Shallow seismic velocity structure of the Chicxulub crater from modeling of Rg dispersion using a genetic algorithm, *Tectonophysics,* **338,** 97–112.

Maguire, P.K.H., Mackenzie, G.D., Denton, P., Trejo, A., Kind, V. & members of the Chicxulub working group, 1998. Preliminary results from a passive seismic array over the Chicxulub impact structure in Mexico, in *Meteorites flux with time and impact effects,* Vol. 140, pp. 177–193, eds Grady, M.M. *et al.,* Geological Society, London, Special Publications.

Matsui, T., Nakano, Y., Horai, K., Wada, K., Tajika, E., Hernandez Zuniga, R. & Campos Enriquez, J.O., 1998. Heatflow anomaly in the Chicxulub crater, *Lunar Planet. Sci. Conf.,* **29,** 1255.

Morgan, J. & Warner, M., 1999a. Chicxulub: the third dimension of a multiring impact basin, *Geology,* **27,** 407–410.

Morgan, J. & Warner, M., 1999b. Morphology of the Chicxulub impact: Peak-ring crater or multi-ring basin?, in *Large Meteorite Impacts and Planetary Evolution,* Vol. 339, pp. 281–290, eds Dressler, B. & Sharpton, V., Spc. Pap. Geol. Soc. Am., Boulder, CO.

Morgan, J., Warner, M. & the Chicxulub Working Group, 1997. Size and morphology of the Chicxulub impact crater, *Nature,* **390,** 472–476.

Morgan, J.V., Christenson, G.L. & Zelt, C.A., 2002. Testing the resolution of a 3D velocity tomogram across the Chicxulub crater, *Tectonophysics,* **355,** 215–226.

Morgan, J.V., Warner, M.R., Collins, G.S., Melosh, H.J. & Christenson, G.L., 2000. Peak-ring formation in large impact craters: geophysical constraints from Chicxulub, *Earth planet. Sci. Lett.,* **183,** 347–354.

Penfield, G.T. & Camargo, Z.A., 1981. Definition of a major igneous zone in the central Yucatan platform with aeromagnetics and gravity. In:, *Abstracts of the 51st Annual Meeting Soc. of Expl. Geophys.,* Abstract, Volume 1, p. 37. Society of Exploration Geophysicists, Tulsa, OK, USA.

Pilkington, M. & Hildebrand, A.R., 2000. Three-dimensional magnetic imaging of the Chicxulub crater, *J. geophys. Res.,* **105,** 23 479–23 491.

Pilkington, M., Hildebrand, A.R. & Ortiz-Alemán, C., 1994. Gravity and magnetic field modeling and structure of the Chicxulub crater, Mexico, *J. geophys. Res.,* **99,** 13 147–13 162.

Ramos-Martínez, J., Chávez-García, F.J., Romero-Jiménez, E., Rodríguez-Zuñiga, J.L. & Gómez-González, J.M., 1997. Site effects in Mexico City: constraints from surface wave inversion of shallow refraction data, *Appl. Geophys.,* **36,** 157–165.

Rebolledo-Vieyra, M., Urrutia-Fucugauchi, J., Marin, L.E., Trejo-García, A. & Sharpton, V.L., 2000. UNAM scientific shallow-drilling program of the Chicxulub impact crater, *Int. Geol. Rev.,* **42,** 928–939.

Shapiro, N., Campillo, M., Paul, A., Singh, S.K., Jongmans, D. & Sánchez-Sesma, F.J., 1997. Surface wave propagation across the Mexican Volcanic Belt and the origin of the long-period seismic-wave amplification in the Valley of Mexico, *Geophys. J. Int.,* **128,** 151–166.

Sharpton, V.L., Dalrymple, G.B., Marín, L.E., Shuraytz, B.C. & Urrutia-Fucugauchi, J., 1992. New links between the Chicxulub impact structure and the Cretaceous/Tertiary boundary, *Nature,* **359,** 819–821.

Sharpton, V.L. *et al.,* 1993. Chicxulub multiring impact basin: Size and other characteristics derived from gravity analysis, *Science,* **261,** 1564–1567.

Sigurdsson, H., Bonte, P., Turpin, L., Chaussidon, M., Metrich, N., Steinberg, M., Pradel, P. & D'Hondt, S., 1991. Geochemical constraints on source region of Cretaceous/Tertiary impact glass, *Nature,* **353,** 839–842.

Snyder, D.B. & Hobbs, R.W., 1999a. Ringed structural zones with deep roots formed by the Chicxulub impact, *J. geophys. Res.,* **104,** 10 743–10 755.

Snyder, D.B. & Hobbs, R.W., 1999b. Deep seismic reflection profiles across the Chicxulub crater, *Geol. Soc. Am. Spec. Paper,* **339,** 263–268

Unsworth, M., Campos-Enríquez, J.O., Belmonte, S., Arzate, J. & Bedrosian, P., 2002. Crustal structure of the Chicxulub impact crater imaged with magnetotelluric exploration, *Geophys. Res. Lett.,* **29**(16), 1788, 10.1029/20026L014998,2002.

Urrutia-Fucugauchi, J., Marín, L. & Sharpton, V.L., 1994. Reverse polarity magnetized melt rocks from the Cretaceous/Tertiary Chicxulub structure, Yucatan peninsula, Mexico, *Tectonophysics,* **237,** 105–112.

Urrutia-Fucugauchi, J., Marín, L. & Trejo-García, A., 1996. UNAM scientific drilling program of Chicxulub impact structure: Evidence for a 300 kilometer crater diameter, *Geophys. Res. Lett.,* **23,** 1565–1568.

Urrutia-Fucugauchi, J., Morán-Zenteno, J., Sharpton, V.L., Buffler, R., Stoeffler, D., & Smit, J., 2001. *The Chicxulub Scientific Drilling Project, Serie: Infraestructura Científica y Desarrollo Tecnológico,* No. 3, Instituto de Geofísica, UNAM, Mexico City, p. 55.

Vermeesch, P. & Morgan, J., 2004. Structure of Chicxulub: Where do we stand?, *Meteoritics and Planetary Science,* in press.